Chapter 3

Design and Analysis of a Novel Wavelength Demultiplexer Based on MMI with Photonic Crystals inside

As mentioned in Chapter 1, the integrated development of photonic devices has become the future trend. For optical telecommunication, much attention has been given to demultiplexing two wavelengths in the 1.3μm and 1.55μm windows and there is a growing interest in the application of multimode interference (MMI) in integrated optics, so we propose a novel 1.3μm and 1.55μm wavelength demultiplexer based on MMI with photonic crystals inside in this chapter. This chapter is organized as follows: Section 3-1 introduction of integrated photonic crystals and the development of photonic crystal applied in integrated optics are presented and discussed. The structure of a novel wavelength demultiplexer based on MMI with photonic crystals inside are designed are described in Section 3-2. Cubic lattice photonic crystal and hexagon lattice photonic crystal including three

patterns, respectively are also briefly derived and discussed in Section 3-2. Simulation resultss of a novel wavelength demultiplexer based on MMI with photonic crystals inside are presented in Section 3-3. We also give the summary and discussions of our designed novel 1.3μm and 1.55μm wavelength demultiplexer with photonic crystals inside in the final Section 3-4.

3-1 Introduction of Integrated Photonic Crystals and Optical Telecommunication

Since the concept of photonic crystal (PhC) structures was introduced by Dr. Yablonovitch in 1987 [69], they have been the focus of intense research in recent years in part because of their potential to realize ultracompact plane lightwave circuits. Novel ideas have been proposed to adjust the photonic crystals for optical communication system.

3-1-1 Introduction of Photonic Crystals

Electromagnetism is the fundamental mediator of all interactions in atomic physics and condensed matter physics, in other words, the force that governs the structure of ordinary matter. In a novel class of engineered

dielectric materials, known as photonic crystals (PhCs) or Photonic Band Gap (PBG) materials, new electromagnetic effects can be obtained. The light localization is a particular interesting phenomenon of fundamental importance for using optical waves in information and communication technologies. Because of the periodic spatial modulation of the dielectric constant, the dispersion equation of the electro-magnetic eigenmodes in photonic crystals are quite different from those in uniform materials. A part from the formation of pass bands and band gaps of eigenfrequencies, extremely small group velocity (the derivative of the angular frequency ω of the radiation field with respect to the wave vector k, $v_g = d\omega/dk$) can be easily obtained in a photonic crystal. In fact a large enhancement of light amplification is obtained when v_g is small, the amplitude amplification factor being proportional to v_g^{-1} [70]. By considering the photonic band structure, given by the normalized frequency $\omega_n = \omega a/2\pi c$ as a function of the wave vector k (a and c being the lattice constant and the light velocity in the vacuo, respectively) of a one-dimensional (1D), or two-dimensional (2D) or three-dimensional (3D) lattice shown in Fig. 3-1, it is possible to find that there exist points, exactly the band gap edges, where v_g is equal to zero. Moreover, the photonic band structure of a 2D or a 3D PhC shows

whole frequency ranges in the Brillouin zone characterized by a small group velocity. This phenomenon, known as the group velocity anomaly, is peculiar to 2D and 3D photonic crystals and it does not occur in 1D periodic structures.

The designed defect in photonic crystals is a very important issue. Most applications of photonic crystals are based on how to introduce the defects into the photonic crystals. By photonic crystals engineering, one can control, trap, or change the wave propagation. Basic photonic crystals defects have two types, point defect and line defect. The material property variation at one point or several points in the periodic structures forms the point defect. For example, in 2D photonic crystals, the usual methods to create defects include removing pillars, filling the holes, or changing the size of pillars or holes, etc. The point defect sometimes behaves like a cavity that has a very high Q factor. The line defects are sometimes treated as photonic crystal waveguide. The way to form line defects in 2D photonic crystals is by removing a line of pillars or filling holes. The wave modes within the photonic bandgap are confined in the photonic crystal waveguide. The bends made by photonic crystal waveguide have proved to be valuable. If the bends and photonic crystals are designed properly,

certain frequency components can propagate with very low loss, even it has 90 degree bend [71]. In addition, some new physical phenomena appeared because of the photonic crystal structures. Negative refractive index, named left handed materials as well, was realized by periodic array of split ring resonators and continuous wires [72]. The optical diode, which has a unidirectional property, was demonstrated by nonlinear photonic crystals [73]. The photonic crystal products have been growing rapidly. After the early applications of highly reflecting mirrors and optical filters, the modern semiconductor lasers, photonic crystal fibers and high efficient LED emerge in the photonic market. Some applications of photonic crystals are shown in Fig. 3-2.

3-1-2 Introduction of Plan Wave Expansion Method

Apparently, the engineering perspective of PhC devices requires development of reliable design tools. As it is well known, the first theories of PhCs were based on the solid-state physics and band-theory for semiconductor materials. Due to the vector nature of electromagnetic (e.m.) fields, these early analyses proved their inaccuracy so mathematical tools, incorporating the vector nature of FM fields, have been developed. A

largely used technique, which gives resultss with good agreement with the experimental ones, is the Plane Wave Method (PWM) where an infinite period lattice is assumed. This method is no longer valid when a linear defect or a point defect is included in the lattice or when a finite period lattice is considered.

The PWM is illustrated in several papers [74]. Here, we summarize the theory very briefly. Maxwell's equations in a transparent, time-invariant, source free and non-permeable ($\mu=\mu_0$) space can be rewritten as Helmholz's equation [75]:

$$\nabla \times \frac{1}{\varepsilon(r)} \nabla \times H(r) = \frac{\omega^2}{c^2} H(r) \tag{3-1}$$

where ε(r) is the dielectric function, ω is the angular frequency and c is the speed of light in vacuum.

In an infinite periodic photonic crystal, using Bloch's theorem [75], a mode in a periodic structure can be expanded as a sum of infinite number of plane waves:

$$\vec{H}(r) = \sum_{G,\lambda} h_{G,\lambda \hat{e}_\lambda} e^{i(\vec{K}+\vec{G})\vec{r}} \tag{3-2}$$

where λ=1, 2, $\vec{k}$ is the wave vector of the plane wave, $\vec{G}$ is the reciprocal lattice vector, $\hat{e}_\lambda$ represents the two unit axis perpendicular to the propagation direction $\vec{K}+\vec{G}$. $\hat{e}_1, \hat{e}_2, \vec{k}+\vec{G}$ are perpendicular to each

other. $h_{G,\lambda}$ is the coefficient of the H component along the axes $\hat{e}_\lambda$.

Using the Fourier transform, the dielectric function can be written as:

$$\varepsilon(r)=\sum_{\vec{G}}\varepsilon_{G}e^{i\vec{G}\cdot\vec{r}} \qquad \varepsilon_G=\frac{1}{V}\iiint_{\Omega}\varepsilon(r)e^{-i\vec{G}\cdot\vec{r}}d\Omega \tag{3-3}$$

where Ω is the unit cell and V is the volume of the unit cell.

Finally, Helmholz's equation can be transformed to an algebraic form [76]:

$$\sum_{G'}\left|\vec{k}+\vec{G}\right|\left|\vec{K}+\vec{G}\right|\varepsilon^{-1}\left(\vec{G}-\vec{G}'\right)\begin{bmatrix}\hat{e}_2\cdot\hat{e}_2' & -\hat{e}_2\cdot\hat{e}_1\\ -\hat{e}_1\cdot\hat{e}_2' & \hat{e}_1\cdot\hat{e}_1'\end{bmatrix}\begin{bmatrix}h_1,G\\ h_2,G\end{bmatrix} \tag{3-4}$$

This is a standard eigenvalue problem and it can be solved using a standard eigen-solver, For 1D and 2D cases, the equation can be simplified. Plane wave expansion method has widely been accepted and used in photonic crystal literature.

3-2 Design a Novel Wavelength Demultiplexer Based on MMI with Photonic Crystals inside

Wavelength division multiplexing (WDM) technology can be used to increase information capacity in transmission systems. In this section, we demonstrate the design of a novel SOI-based MMI demultiplexer for 1.3μm and 1.55μm operation by filled photonic crystals structure using our designed 2x2 MMI device in Chapter 2. We put photonic crystals which are

component of period hole filled GaAs into multimode interference region. The region of photonic crystals is located in the center of multimode interference region. Fig. 3-3 show our designed structure of wavelength demultiplexer based on MMI with photonic crystals inside and detail designs are demonstrated in section 3-2-1 and 3-2-2.

3-2-1 Cubic Lattice Photonic Crystals in MMI Region including Three Pattern

We use our designed 2x2 MMI device which size is L_{MMI}=29.3μm, W_{MMI}=2.4μm and access waveguide w=400nm. In this section, we demonstrate cubic lattice at center of MMI region including circle pattern, square pattern and hexagonal pattern. In our designed 2-D circle pattern of cubic lattice photonic crystals has 10 holes filled GaAs in X axis and 4 holes filled GaAs in Y axis, then the structure is shown in Fig. 3-4. This circle hole-to-hole distance is defined as lattice=a and the size of circle hole is defined as width=w, and they have been discussed in section 3-3. In our designed 2-D square pattern of cubic lattice photonic crystals has 10 holes filled GaAs in X axis and 4 holes filled GaAs in Y axis, then the structure is shown in Fig. 3-5. This square hole-to-hole distance is defined as lattice=a

and the size of square hole is defined as width=w and they have been discussed in section 3-3. In our designed 2-D hexagonal pattern of cubic lattice photonic crystals has 10 holes filled GaAs in X axis and 4 holes filled GaAs in Y axis, then the structure is shown in Fig. 3-6. This hexagonal hole-to-hole distance is defined as lattice=a and the size of hexagonal hole is defined as width=w, and they have been discussed in section 3-3.

3-2-2 Hexagonal Lattice Photonic Crystals in MMI Region including Three Pattern

We use our designed 2x2 MMI device which size is L_{MMI}=29.3μm, W_{MMI}=2.4μm and access waveguide w=400nm. In this section, we demonstrate hexagonal lattice at center of MMI region including circle pattern, square pattern and hexagonal pattern. In our designed 2-D circle pattern of hexagon lattice photonic crystals has 10 holes filled GaAs in X axis and 4 holes filled GaAs in Y axis, then the structure is shown in Fig. 3-7. This circle hole-to-hole distance is defined as lattice=a and the size of circle hole is defined as width=w, and they have been discussed in section 3-3. In our designed 2-D square pattern of hexagonal lattice photonic

crystals has 10 holes filled GaAs in X axis and 4 holes filled GaAs in Y axis, then the structure is shown in Fig. 3-8. This square hole-to-hole distance is defined as lattice=a and the size of square hole is defined as width=w, and they have been discussed in section 3-3. In our designed 2-D hexagonal pattern of hexagonal lattice photonic crystals has 10 holes filled GaAs in X axis and 4 holes filled GaAs in Y axis, then the structure is shown in Fig. 3-9. This hexagonal hole-to-hole distance is defined as lattice=a and the size of hexagonal hole is defined as width=w, and they have been discussed in section 3-3.

3-3 Simulation results of a Novel Wavelength Demultiplexer Based on MMI with Photonic Crystals inside

In this section, we demonstrate the simulation results of various combinations. The performance of the demultiplexer mainly by the contrast ratio which is defined as [8]:

$C = 10\log\frac{P_1}{P_2}$ and P_1 is output 1, P_2 is output 2

The photonic crystals effecting the change of multimode interference is designed for dividing two different optical signals with wavelength λ_1 =

1300 nm and λ_2 = 1550 nm, which are incident simultaneously on the input 1. We lay out all the parameters in Table IV and Table V.

3-3-1 Simulation results of lattice=300nm and width=100nm, 125nm, 150nm, 175nm and 200nm

The simulation results of contrast ratio of cubic lattice=300nm and width of circle, square and hexagonal pattern with width =100nm, 125nm, 150nm, 175nm and 200nm are between -1.0704dB and -3.9895dB, when input wavelength is 1.3μm. The simulation results of contrast ratio of cubic lattice=300nm and width of circle, square and hexagonal pattern with width =100nm, 125nm, 150nm, 175nm and 200nm are between 1.0733dB and 3.7595dB, when input wavelength is 1.55μm.

The simulation results of contrast ratio of hexagonal lattice=300nm and width of circle, square and hexagonal pattern with width =100nm, 125nm, 150nm, 175nm and 200nm are between -1.0704dB and -3.9895dB, when input wavelength is 1.3μm. The simulation results of contrast ratio of hexagonal lattice=300nm and width of circle, square and hexagonal pattern with width =100nm, 125nm, 150nm, 175nm and 200nm are between 1.0733dB and 3.7595dB, when input wavelength is 1.55μm.

3-3-2 Simulation results of lattice=400nm and width=100nm, 125nm, 150nm, 175nm and 200nm

The simulation results of contrast ratio of cubic lattice=400nm and width of circle, square and hexagonal pattern with width =100nm, 125nm, 150nm, 175nm and 200nm are between -1.7644dB and -9.4672dB, when input wavelength is 1.3μm. The simulation results of contrast ratio of cubic lattice=400nm and width of circle, square and hexagonal pattern with width =100nm, 125nm, 150nm, 175nm and 200nm are between 2.6434dB and 5.6368dB, when input wavelength is 1.55μm.

The simulation results of contrast ratio of hexagonal lattice=400nm and width of circle, square and hexagonal pattern with width =100nm, 125nm, 150nm, 175nm and 200nm are between -3.6645dB and -9.4672dB, when input wavelength is 1.3μm. The simulation results of contrast ratio of hexagonal lattice with width =400nm and width of circle, square and hexagonal pattern=100nm, 125nm, 150nm, 175nm and 200nm are between 2.9744dB and 5.4144dB, when input wavelength is 1.55μm.

3-3-3 Simulation results of lattice=500nm and width=100nm, 125nm, 150nm, 175nm and 200nm

The simulation results of contrast ratio of cubic lattice=500nm and width of circle, square and hexagonal pattern with width =100nm, 125nm, 150nm, 175nm and 200nm are between -7.8241dB and -15.6215dB, when input wavelength is 1.3μm. The simulation results of contrast ratio of cubic lattice=500nm and width of circle, square and hexagonal pattern with width =100nm, 125nm, 150nm, 175nm and 200nm are between 4.8972dB and 8.3623dB, when input wavelength is 1.55μm.

The simulation results of contrast ratio of hexagonal lattice=500nm and width of circle, square and hexagonal pattern with width =100nm, 125nm, 150nm, 175nm and 200nm are between -10.7223dB and -12.2598dB, when input wavelength is 1.3μm. The simulation results of contrast ratio of hexagonal lattice=500nm and width of circle, square and hexagonal pattern with width =100nm, 125nm, 150nm, 175nm and 200nm are between 5.6233dB and 9.7919dB, when input wavelength is 1.55μm.

3-3-4 Simulation results of lattice=600nm and width=100nm, 125nm, 150nm, 175nm and 200nm

The simulation results of contrast ratio of cubic lattice=600nm and width of circle, square and hexagonal pattern with width =100nm, 125nm,

150nm, 175nm and 200nm are between -16.7499dB and -23.7343dB, when input wavelength is 1.3μm. The simulation results of contrast ratio of cubic lattice=600nm and width of circle, square and hexagonal pattern with width =100nm, 125nm, 150nm, 175nm and 200nm are between 10.0794dB and 12.8096dB, when input wavelength is 1.55μm.

The simulation results of contrast ratio of hexagonal lattice=600nm and width of circle, square and hexagonal pattern with width =100nm, 125nm, 150nm, 175nm and 200nm are between -13.9083dB and -15.5664dB, when input wavelength is 1.3μm. The simulation results of contrast ratio of hexagonal lattice=600nm and width of circle, square and hexagonal pattern with width =100nm, 125nm, 150nm, 175nm and 200nm are between 7.1902dB and 11.7967dB, when input wavelength is 1.55μm.

3-4 Discussion and Summary

We have arranged simulation results of lattice=300nm and width=100nm, 125nm, 150nm, 175nm and 200nm in Table VI. We have arranged simulation results of lattice=400nm and width=100nm, 125nm, 150nm, 175nm and 200nm in Table VII. We have arranged simulation results of lattice=500nm and width=100nm, 125nm, 150nm, 175nm and

200nm in Table VIII. We have arranged simulation results of lattice=600nm and width=100nm, 125nm, 150nm, 175nm and 200nm in Table IX. By the simulation results of section 3-3 we can find the best parameters range of a novel wavelength demultiplexer based on MMI with photonic crystals inside when the lattice is cubic lattice=600nm, the pattern is circle pattern, hence the range have been discussed. Fig. 3-10~Fig. 3-14 show the bend structure at cubic lattice=600nm, circle pattern and width=100nm, 125nm, 150nm, 175nm and 200nm.The contrast ratio has been compared in Fig. 3-15 and Fig. 3-16, so the best width=100nm has been found. Insertion loss of all is around 3dB. The optical field is shown in Fig. 3-17 at input wavelength=1.3μm. The optical field is shown in Fig. 3-18 at input wavelength=1.55μm. We have proposed the optimum parameters of a novel device which the contrast ratio is -18.9325dB at input wavelength=1.3μm, the contrast ratio is 12.8096dB at input wavelength=1.55μm.

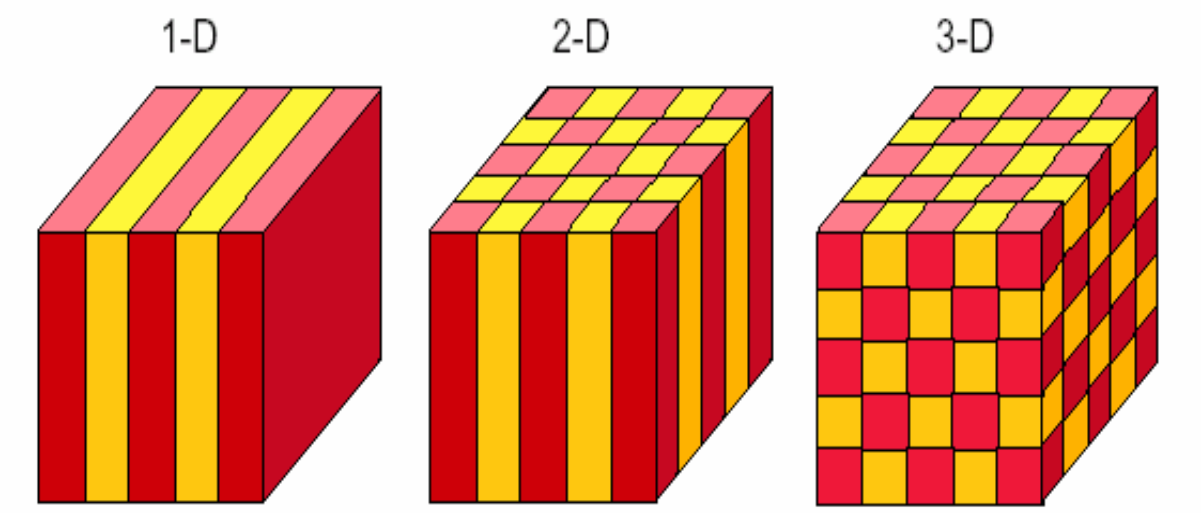

(a) (b) (c)

Fig 3-1 Three type of photonic crystals (a) one dimension (b) two dimension (c) three dimension

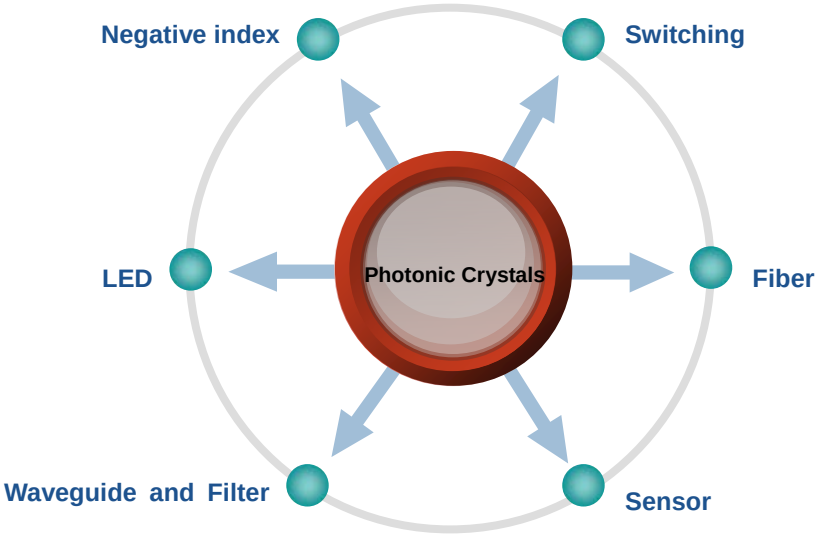

Fig 3-2 Applications of the photonic crystals

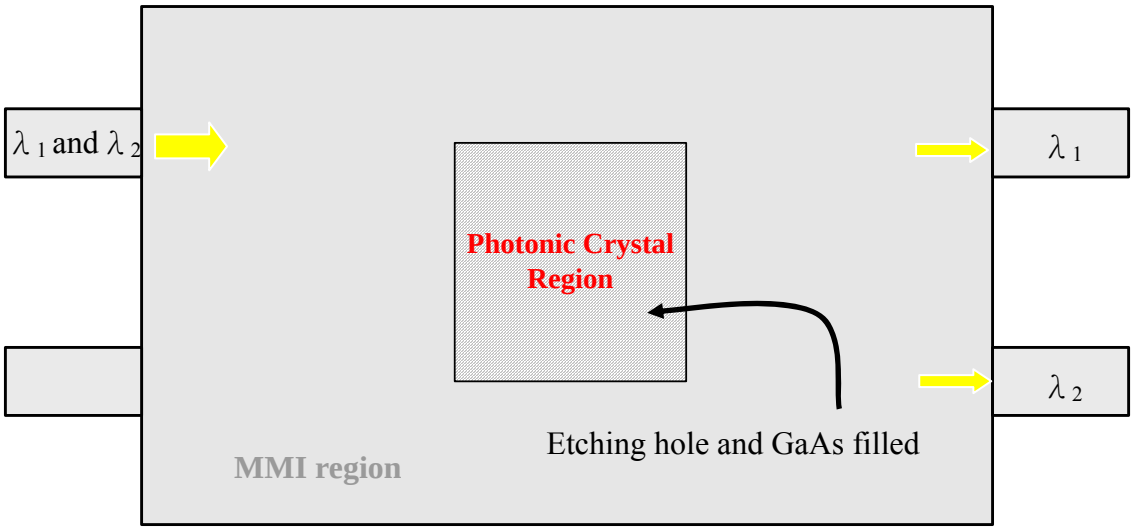

Fig 3-3 A novel wavelength demultiplexer based on MMI with photonic crystals inside

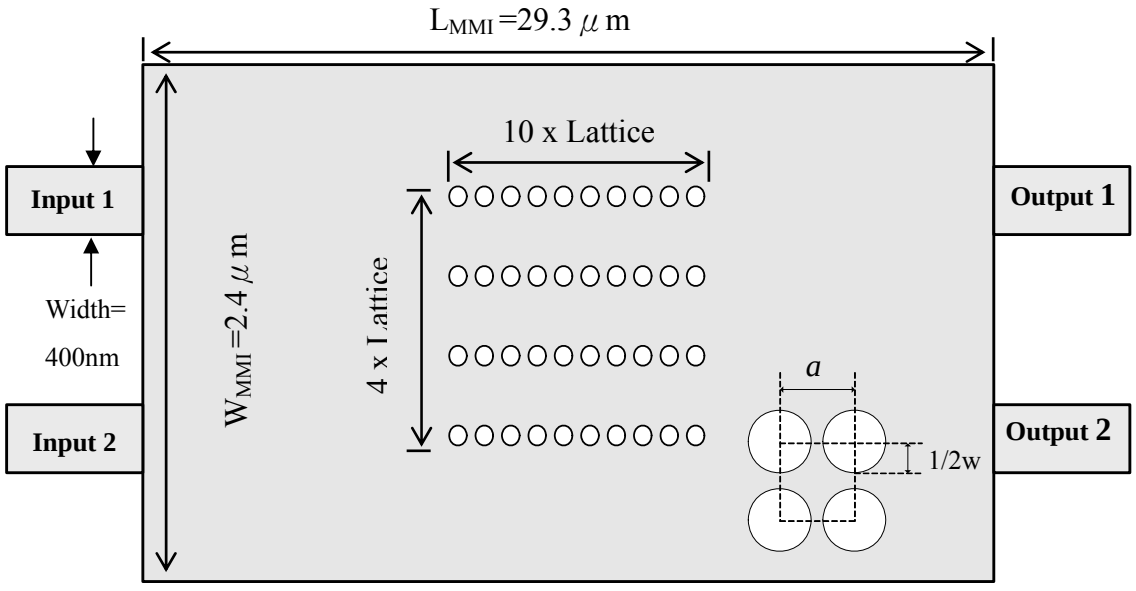

Fig 3-4 A novel wavelength demultiplexer based on MMI with cubic lattice and circle pattern photonic crystals inside

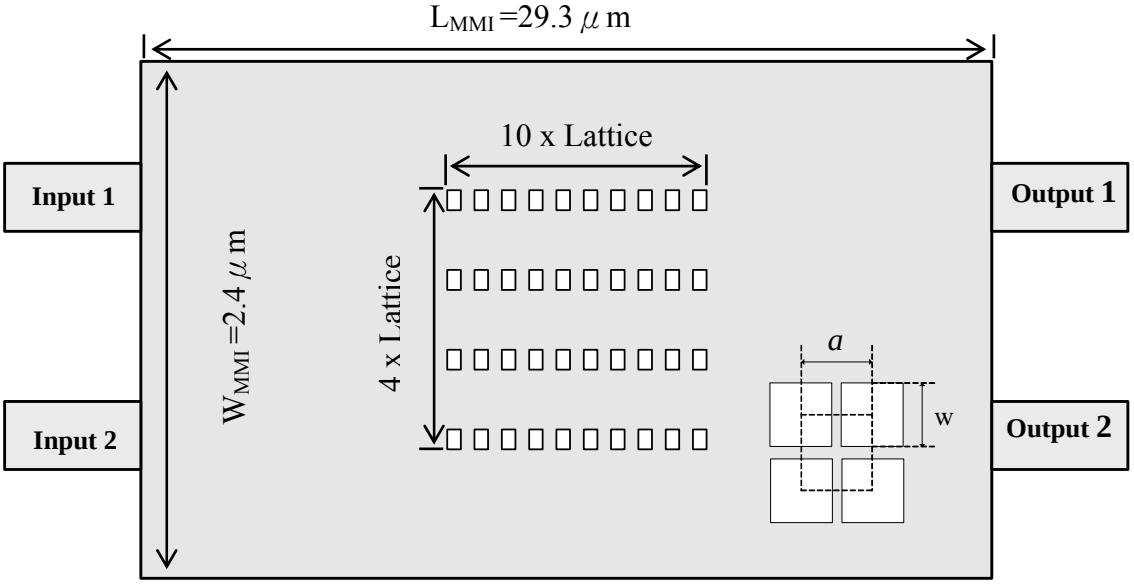

Fig 3-5 A novel wavelength demultiplexer based on MMI with cubic lattice and square pattern photonic crystals inside

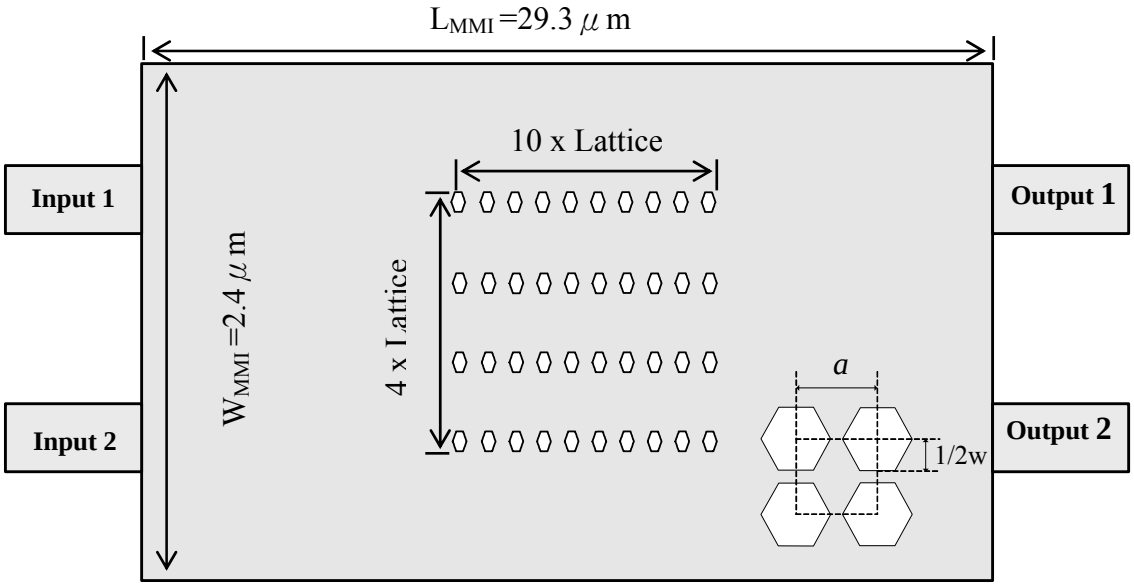

Fig 3-6 A novel wavelength demultiplexer based on MMI with cubic lattice and hexagonal pattern photonic crystals inside

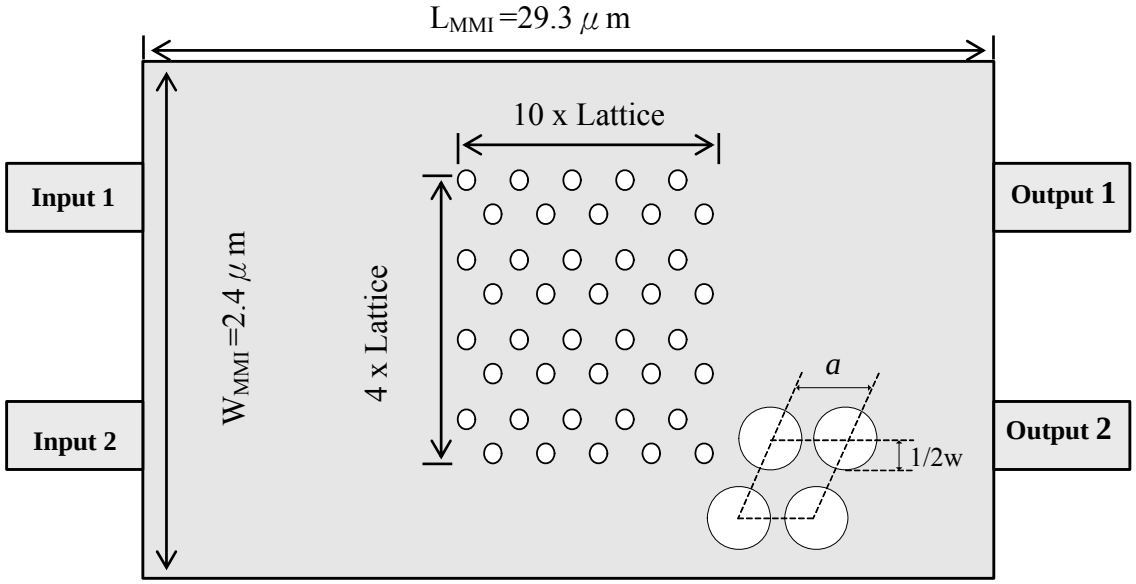

Fig 3-7 A novel wavelength demultiplexer based on MMI with hexagonal lattice and circle pattern photonic crystals inside

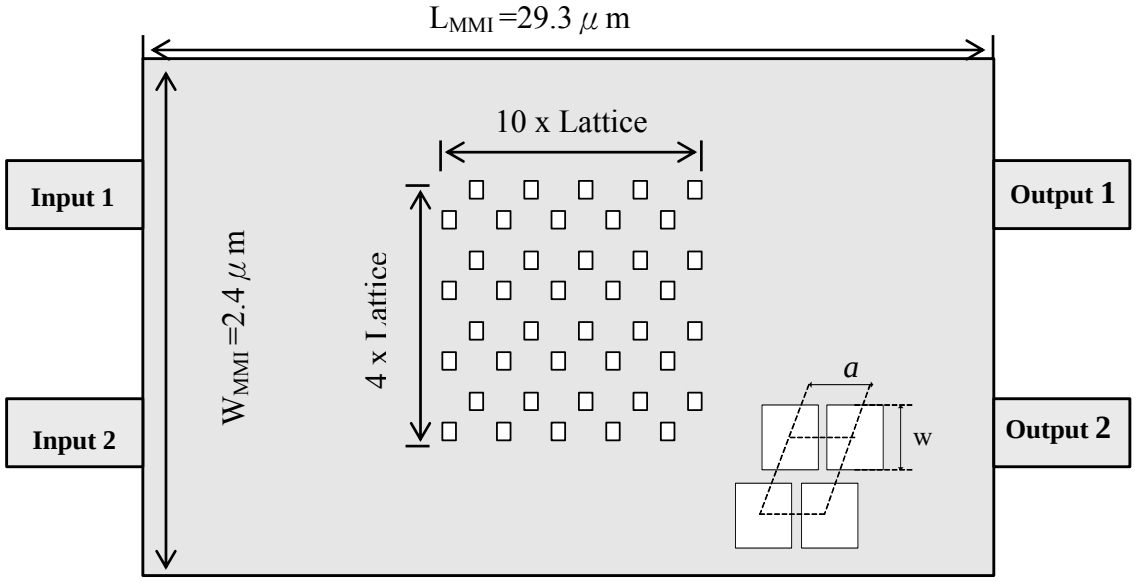

Fig 3-8 A novel wavelength demultiplexer based on MMI with hexagonal lattice and square pattern photonic crystals inside

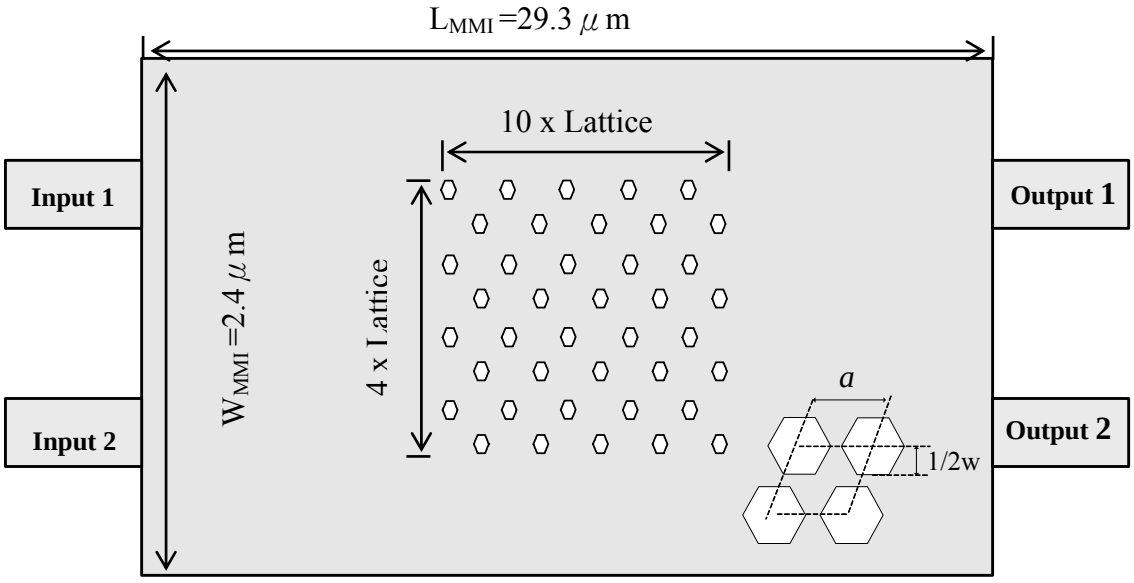

Fig 3-9 A novel wavelength demultiplexer based on MMI with hexagonal lattice and hexagonal pattern photonic crystals inside

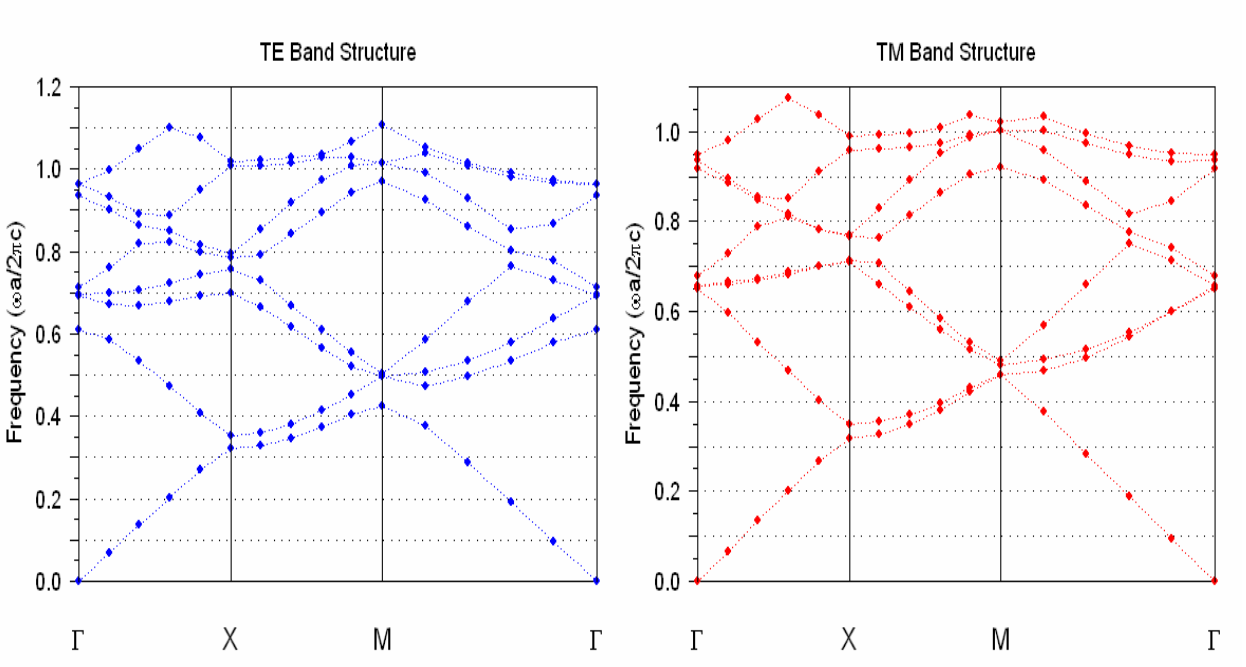

Fig.3- 10 TE and TM photonic band structure of cubic lattice=600nm and circle width=100nm

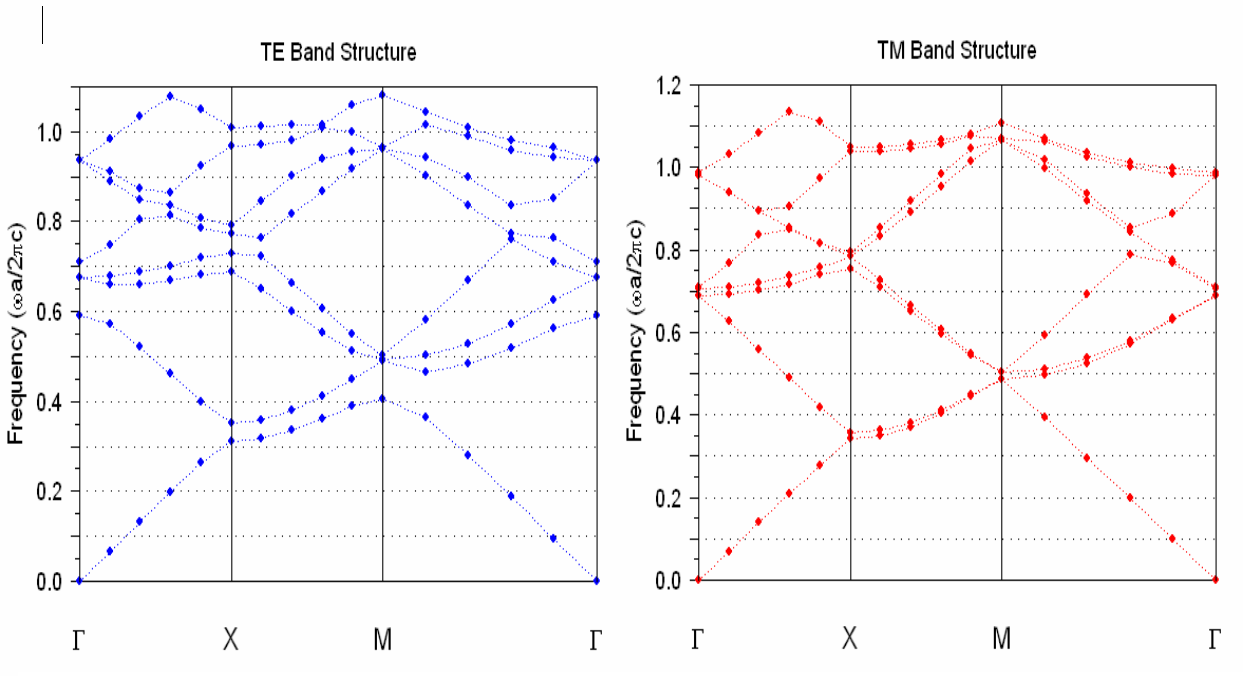

Fig.3-11 TE and TM photonic band structure of cubic lattice=600nm and circle width=125nm

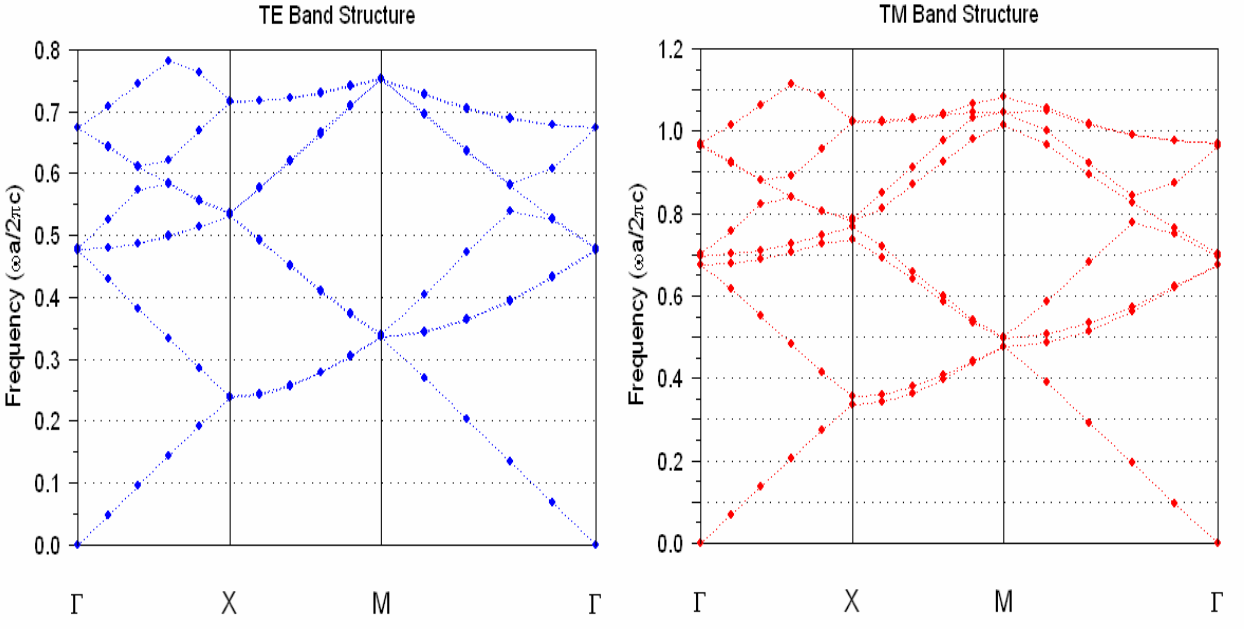

Fig.3-12 TE and TM photonic band structure of cubic lattice=600nm and circle width=150nm

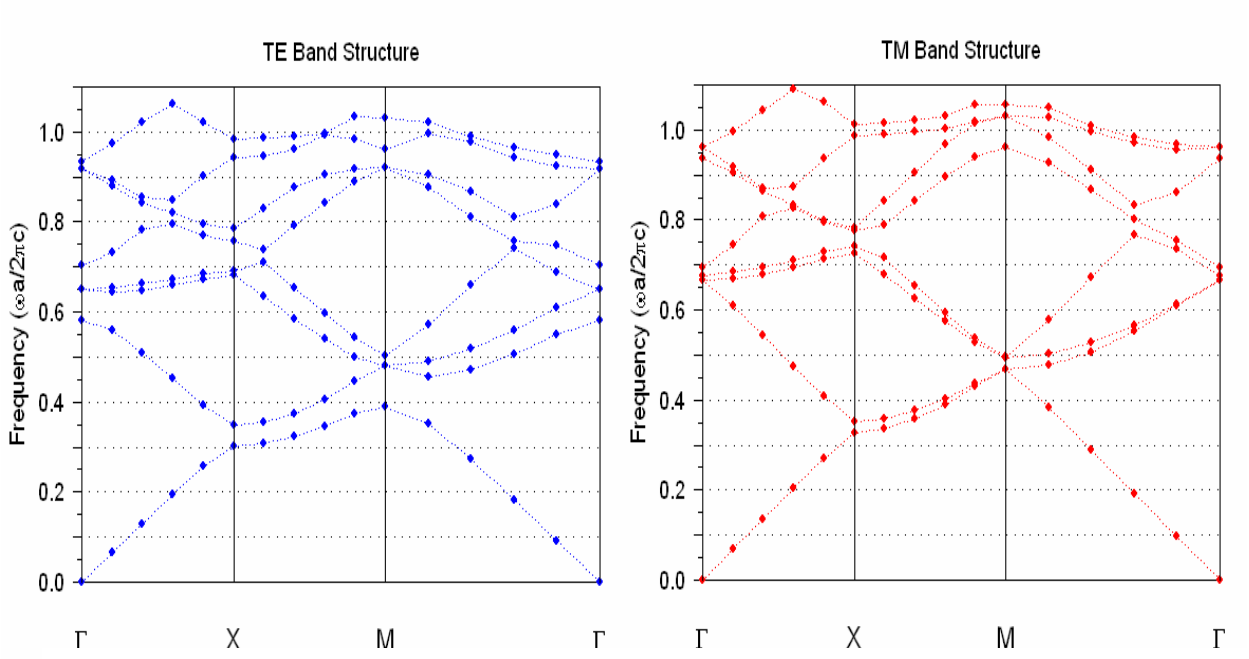

Fig.3-13 TE and TM photonic band structure of cubic lattice=600nm and circle width=175nm

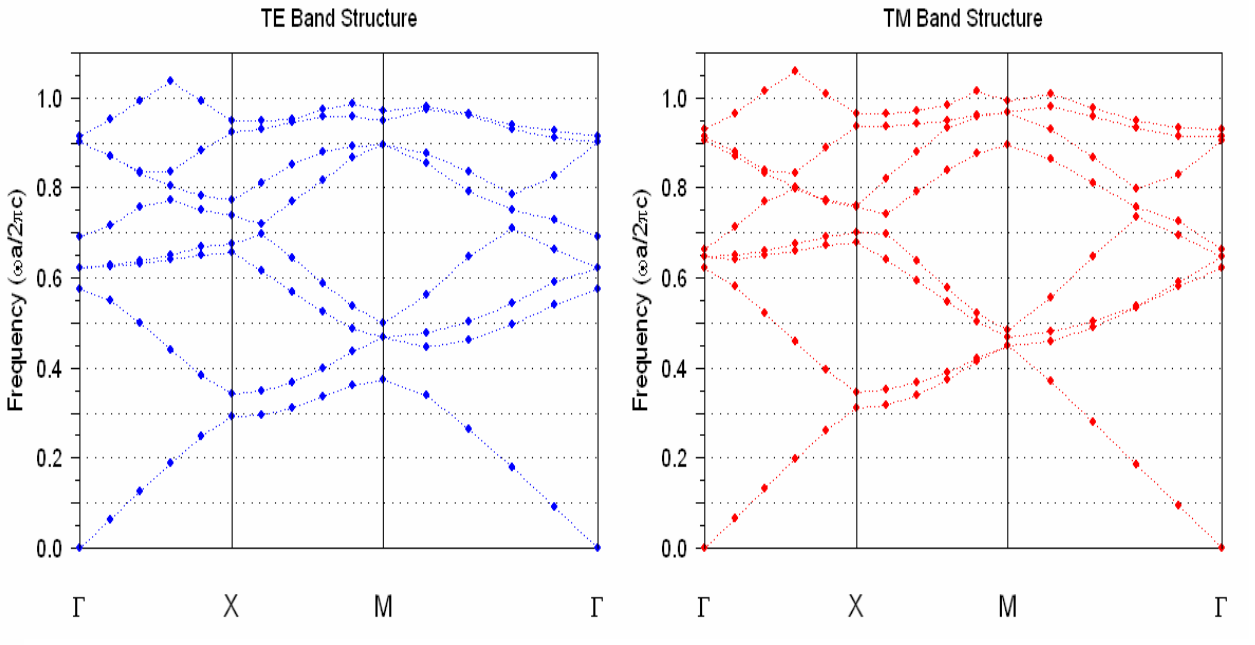

Fig.3-14 TE and TM photonic band structure of cubic lattice=600nm and circle width=200nm

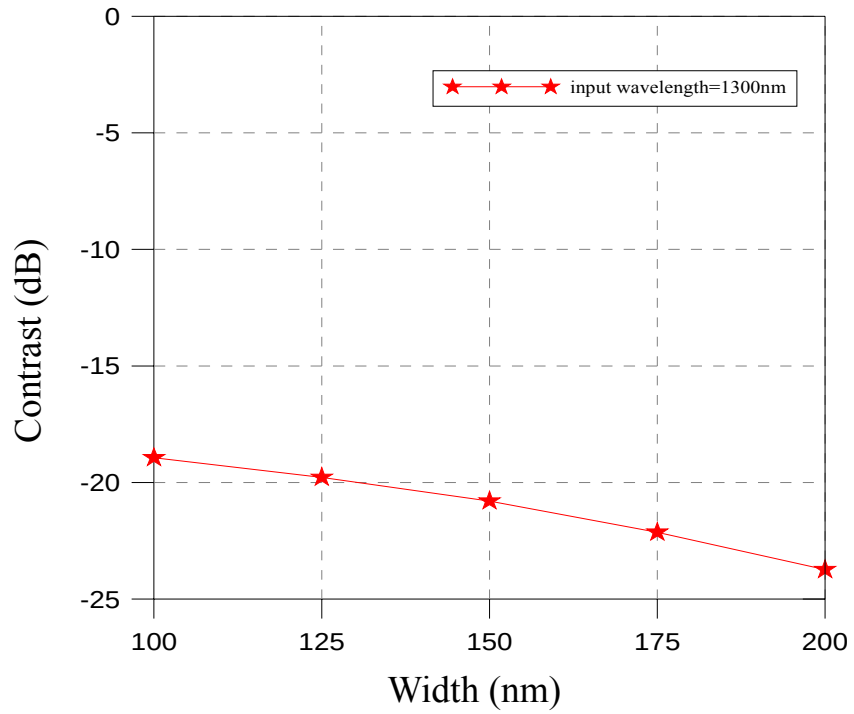

Fig.3-15 Contrast ratio of various width at cubic lattice=600nm and input wavelength=1.3μm

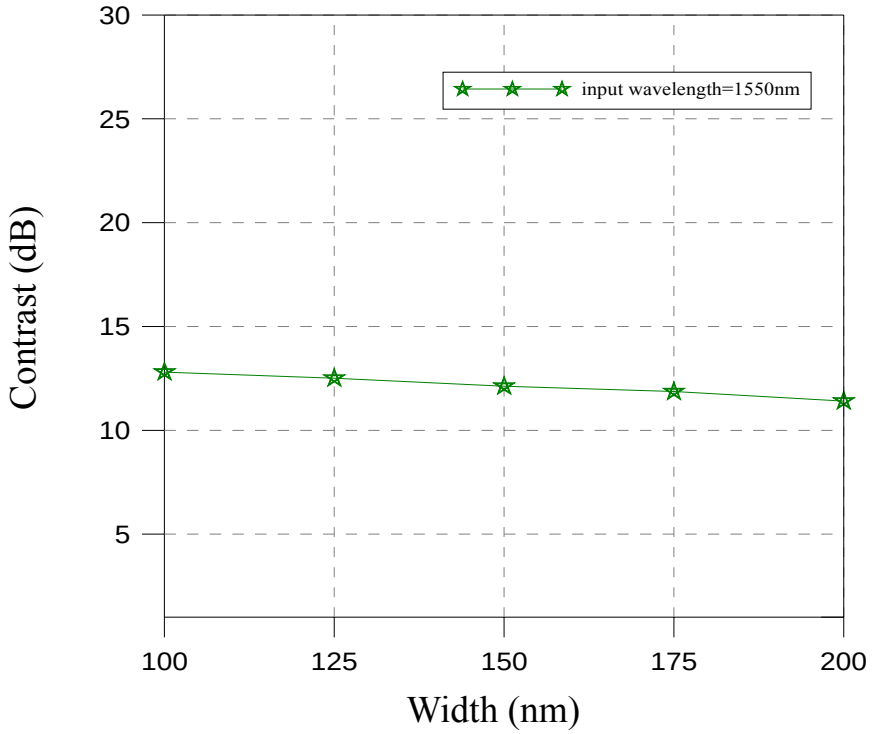

Fig.3-16 Contrast ratio of various width at cubic lattice=600nm and input wavelength=1.55μm

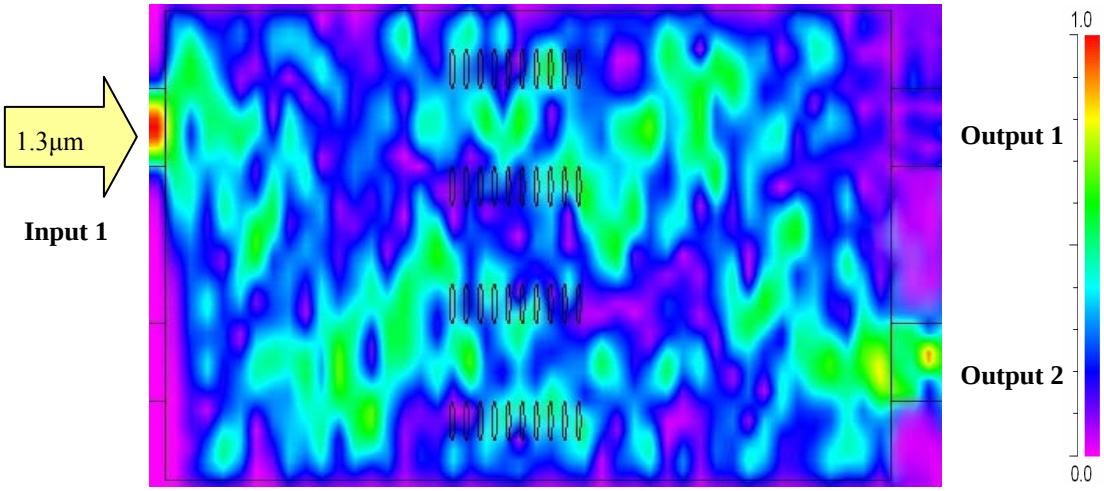

Fig.3-17 Optical field of a novel wavelength demultiplexer based on MMI with photonic crystals inside at input wavelength=1.3μm

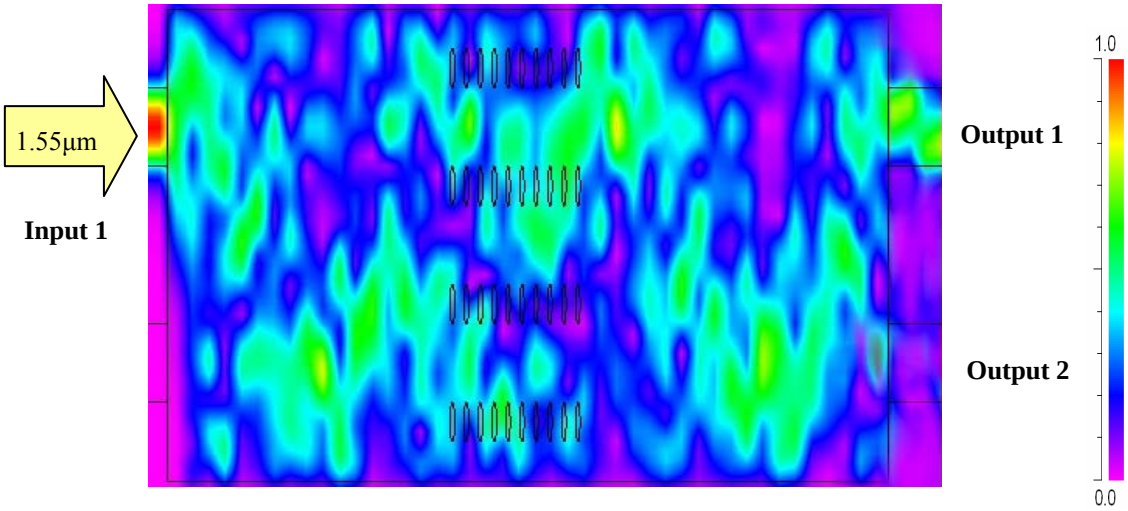

Fig.3-18 Optical field of a novel wavelength demultiplexer based on MMI with photonic crystals inside at input wavelength=1.55μm

Table IV Summary of lattice and pattern

Lattice	Pattern
Cubic	circle
	square
	hexagonal
Hexagon	circle
	square
	hexagonal

Table V Summary of size of lattice and width

Lattice/Width (nm)				
300/100	300/125	300/150	300/175	300/200
400/100	400/125	400/150	400/175	400/200
500/100	500/125	500/150	500/175	500/200
600/100	600/125	600/150	600/175	600/200

Table VI Summary of simulation results of lattice=300nm and width=100nm, 125nm, 150nm, 175nm and 200nm

Lattice= 300nm	Pattern	Size (nm)	Contrast (dB)	
			Input wavelength=1.3 μm	Input wavelength=1.55 μm
Cubic	circle	100	-3.8842	2.0423
		125	-3.2324	2.0158
		150	-3.5158	1.1652
		175	-3.8316	1.4784
		200	-3.1474	1.9415
	square	100	-3.4632	3.5452
		125	-3.7794	2.2764
		150	-3.0948	1.1224
		175	-3.4105	1.0733
		200	-3.7263	2.1204
	hexagonal	100	-3.0421	2.2554
		125	-3.3579	2.4708
		150	-3.6737	3.7595
		175	-3.9895	3.1151
		200	-3.3053	3.5387
Hexagon	circle	100	-3.6211	5.0041
		125	-3.9369	4.5167
		150	-3.2527	4.0578
		175	-3.5684	3.6153
		200	-3.8842	3.2792
	square	100	-1.0704	5.0591
		125	-1.5738	3.2299
		150	-2.1558	3.8994
		175	-2.3879	3.6369
		200	-3.3191	3.7618
	hexagonal	100	-3.6768	5.3661
		125	-3.6501	4.6309
		150	-3.2201	4.5483
		175	-2.3873	5.7474
		200	-1.3974	4.7933

Table VII Summary of simulations result of lattice=400nm and width=100nm, 125nm, 150nm, 175nm and 200nm

Lattice= 400nm	Pattern	Size (nm)	Contrast (dB)	
			Input wavelength=1.3 μm	Input wavelength=1.55 μm
Cubic	circle	100	-3.5204	5.6368
		125	-3.8158	5.4620
		150	-3.7637	5.2480
		175	-3.3001	5.0746
		200	-2.0818	4.7460
	square	100	-3.6973	5.5184
		125	-3.8965	5.3463
		150	-3.7209	5.1680
		175	-3.0847	4.8442
		200	-1.7644	4.5203
	hexagonal	100	-3.6938	5.1367
		125	-8.4942	3.5610
		150	-6.7810	3.1923
		175	-5.9397	3.0807
		200	-3.7797	2.6434
Hexagon	circle	100	-3.6645	5.5032
		125	-4.0883	5.2476
		150	-4.4695	4.9781
		175	-4.6964	4.6385
		200	-4.6357	4.2139
	square	100	-3.8213	5.4144
		125	-4.2246	5.1736
		150	-4.6075	4.8709
		175	-4.7143	4.4729
		200	-4.4559	4.0224
	hexagonal	100	-9.4672	4.9961
		125	-7.8685	3.7968
		150	-6.7517	3.5461
		175	-5.4835	3.3203
		200	-4.1086	2.9744

Table VIII Summary of simulations result of lattice=500nm and width=100nm, 125nm, 150nm, 175nm and 200nm

Lattice= 500nm	Pattern	Size (nm)	Contrast (dB)	
			Input wavelength=1.3 μm	Input wavelength=1.55 μm
Cubic	circle	100	-13.4263	6.8385
		125	-13.9166	6.7123
		150	-14.5244	6.5214
		175	-14.9671	6.3194
		200	-15.5185	6.1098
	square	100	-13.5392	6.6877
		125	-14.0477	6.5295
		150	-14.5992	6.3390
		175	-15.1651	5.1104
		200	-15.6215	4.8972
	hexagonal	100	-10.6747	7.4249
		125	-9.7307	6.8052
		150	-9.0085	7.4805
		175	-8.6959	8.3623
		200	-7.8241	6.0005
Hexagon	circle	100	-12.2598	5.6233
		125	-11.9567	8.4874
		150	-11.6154	9.2895
		175	-11.2859	9.0733
		200	-10.8564	9.8901
	square	100	-12.1458	9.5847
		125	-11.8623	8.4147
		150	-11.5057	7.1958
		175	-11.0786	8.0778
		200	-10.7223	9.7919
	hexagonal	100	-12.0251	8.2980
		125	-11.6758	6.9081
		150	-11.5637	5.7833
		175	-12.2089	6.5123
		200	-11.1166	8.3515

Table IX Summary of simulations result of lattice=600nm and width=100nm, 125nm, 150nm, 175nm and 200nm

Lattice= 600nm	Pattern	Size (nm)	Contrast (dB)	
			Input wavelength=1.3 μm	Input wavelength=1.55 μm
Cubic	circle	100	-18.9325	12.8096
		125	-19.0767	12.5095
		150	-20.7899	12.1250
		175	-22.1338	11.8691
		200	-22.7343	11.4113
	square	100	-18.9209	10.5974
		125	-19.7053	10.4503
		150	-20.3084	10.3090
		175	-20.9643	10.0794
		200	-21.7135	10.9064
	hexagonal	100	-17.3042	10.4383
		125	-17.2429	11.9254
		150	-16.5342	11.7892
		175	-16.7513	11.7603
		200	-16.7499	10.6785
Hexagon	circle	100	-15.5664	11.0041
		125	-15.9307	12.1535
		150	-14.1035	9.3107
		175	-15.3982	10.4932
		200	-14.3322	11.7967
	square	100	-15.3471	8.0390
		125	-14.6634	9.1852
		150	-14.9089	10.3603
		175	-14.9643	11.6450
		200	-13.9083	10.9443
	hexagonal	100	-14.5376	7.6217
		125	-14.0834	6.8933
		150	-15.5189	7.5237
		175	-15.5621	7.8286
		200	-15.7047	7.1902